Bender performance for Hard X-ray Single-shot Spectrometer of European XFEL Diagnostics

Karina Kazarian

Moscow State University, Moscow, Russia

Supervisor:

Dr. Naresh Gandhi Kujala

Scientist, X-ray Photon Diagnostics Group

European XFEL, Schenefeld, Germany

September 6, 2017

Abstract

European X-ray Free-Electron Laser (XFEL) facility is the world brightest source which is constructed in Hamburg Germany. It is starting the user operation at the beginning of Sep'2017. It will generate 27000 X-ray pulses per second. It is based on self-amplified spontaneous emission (SASE) method for generation of extremely short pulses in the range of 10 – 100fs. Due to its stochastic nature, the pulses fluctuate both in intensity and spectral. An in-situ photon diagnostics tool that provides well-resolved spectral measurements of each individual pulse without compromising the quality of the beam delivered to the experiment is needed to mitigate the effects of these fluctuations on experimental results. One of such instruments which will soon be used in the SASE1 beamline is the high resolution hard X-ray single-pulse diagnostic spectrometer (HIREX). HIREX spectrometer is an on-line device, based on a diamond diffraction grating used in transmission to split off a small fraction (0.1%) of the photon beam, a bent crystal as a dispersive element, and a MHz-repetition rate strip detector. It is using a set of four static bend crystal holders each of fixed radius. Since XFEL beam has a wide continuous energy range the discrete set of radii limits the quality of the spectrometer operation on any energy.

In this research we present a dynamic bender design which should increase both the energy resolution and flexibility, as well as reduce the adjustment time of the setup. The goal is to demonstrate/compare that the fixed bender will give the same results as dynamic bender.

Contents

1. Introduction

1.1 XFEL pulse structure

European X-ray Free-Electron-Laser (XFEL) is a light source which provides radiation ranging from (0,26 keV)the carbon K-edge to (25 keV) very hard X-rays. It characterized by unique features such as: high average brilliance, extreme peak intensities, very small angstrom resolution, femtosecond pulse duration and high degree of coherence. The European XFEL facility consists of three sections, which are shown in figure 1.

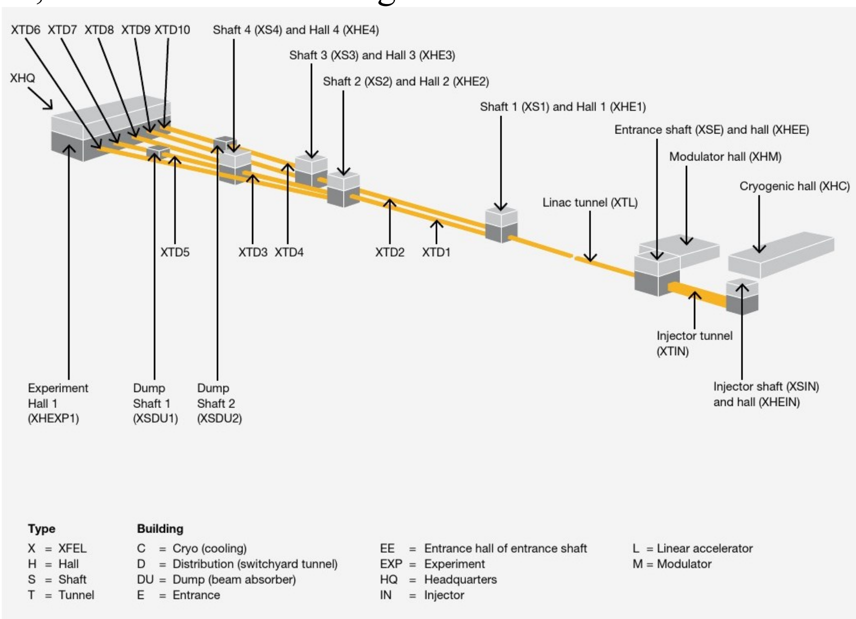

Figure 1: Overall layout of the European XFEL facility. XTD9 tunnel (SASE1) serves two beamlines FXE and SPB/SFX; XTD10 tunnel (SASE3) serves two beamlines SQS and SCS; XTD6 tunnel (SASE2) serves two beamlines HED and MID. (1)

The first section is the superconducting low emittance 17.5 GeV electron accelerator, which downstream distributes to two beam lines containing the FEL undulator sources. It consists of a photo-injector to generate electron bunches by means of the photoelectric effect and the main linac to accelerates the electrons by means of 96 modules. The accelerator is operated so that the pulse comes in trains at a repetition rate of 10 HZ, with maximum 2700 pulses per train. The figure 2 and 3 shows the SASE spectrum and pulse structure.

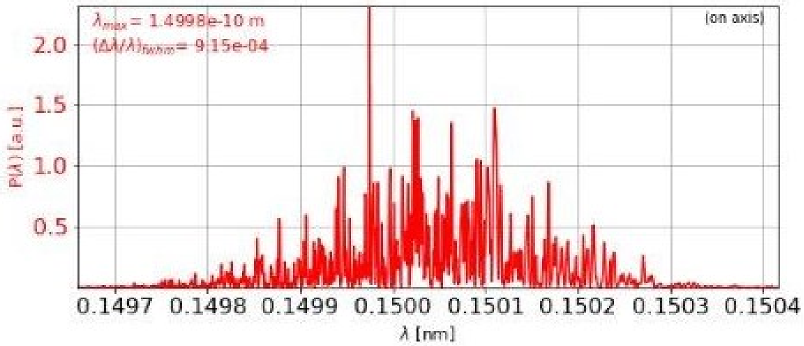

Figure 2: SASE1 pulse simulation at 8 keV. (Courtesy of Gianluca Aldo Geloni)

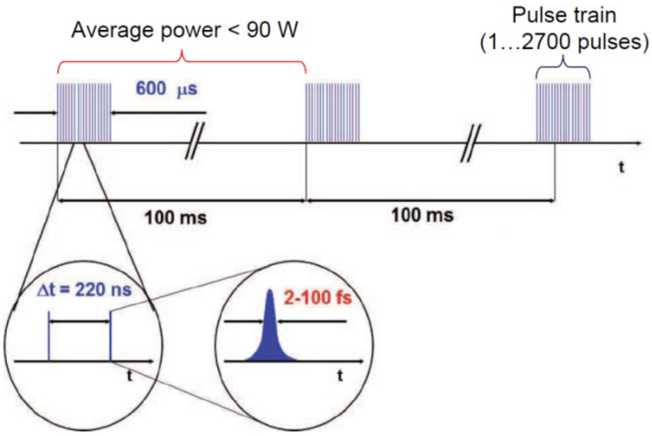

Figure 3: The XFEL pulse structure.

The European XFEL based on self-amplified spontaneous emission (SASE), There are three undulator sources, of which the two called SASE1 and SASE2 provide 3 to 25 keV in the first harmonic, while SASE3 produces the soft X –ray 250eV to 3 keV. There are six experimental hutches, which run for user operation. The Single Particles, Biomolecules and Serial Crystallography (SPB/SFX) scientific instrument's primary goal is to enable three-dimensional imaging, or three-dimensional structure determination, of micrometer-scale and smaller objects. The Femtosecond X-ray Experiment (FXE) scientific instrument has a primary scientific focus in the field of photo-induced chemical dynamics in liquid environments. The SQS (Small Quantum Systems) scientific instrument is dedicated to investigations of fundamental processes of light-matter interaction in the soft X-ray wavelength regime. The Spectroscopy and Coherent Scattering (SCS) aims at time-resolved experiments to unravel the electronic, spin and structural properties of materials in their fundamental space-time dimensions. The Materials Imaging and Dynamics (MID) will provide unique capabilities in ultrafast imaging and dynamics of materials, with particular focus on the application of coherent X-ray scattering and diffraction techniques. The High-Energy Density (HED) instrument aims at the investigation of matter at extreme states of temperature, pressure, density, and/or electromagnetic fields using hard X-ray FEL radiation. (1)

1.2 XFEL Photon Diagnostics devices

X-ray photon diagnostics is essential for monitoring the photon pulse parameters generated by the European XFEL. The diagnostics systems provide information to the machine for setup, operation and optimization of the accelerator, undulator and X-ray optics, especially during commissioning. Diagnostics is also mandatory for normalization and interpretation of the experimental data. The sequence of diagnostics devices in the tunnel XTD2 (SASE1) is illustrated in more detail in the figure 4.

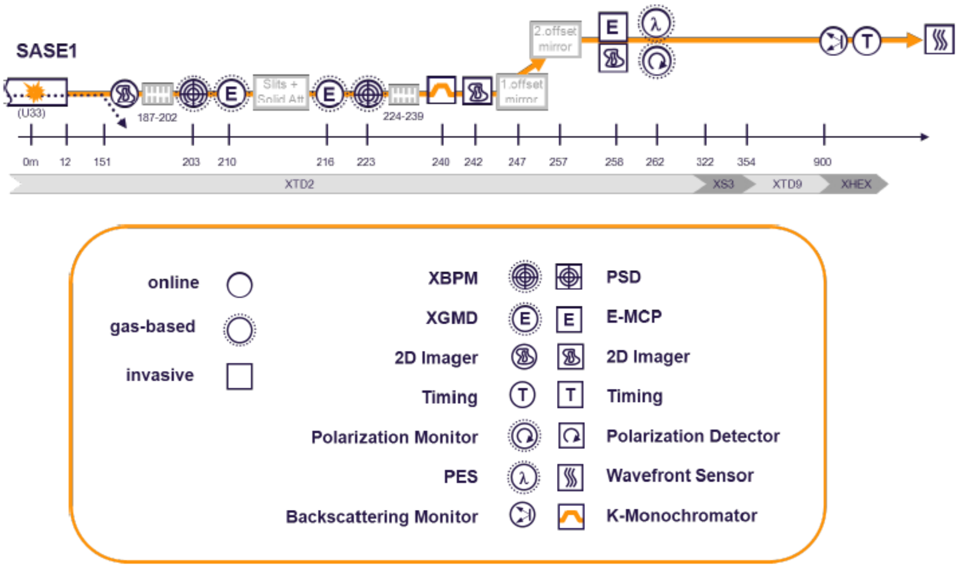

Figure 4: Location of diagnostics devices complete with a legend with symbol descriptions in the SASE1 beamline. (2)

In classification, based on the physical interaction between photon beam and diagnostics devices they are grouped into one of following classes (2): online gas-based devices, online solid-state based devices, invasive devices. Besides spontaneous and FEL radiation requires different properties for example: high photon detection sensitivity and pulse-train heat load capability, respectively. Great contribution to the variety of technics also gives wide energy range. For soft X-rays gas-based methods are preferred to avoid excessive absorption, unlike for hard X-rays the solid targets provide manageable average heat load. All in all there are a lot of both electron and photon beams parameters necessary to monitor continuously: beam position, shot-to-hot wavelength, spectral width, degree and orientation of linear polarization, etc. So that even for a single beam property the diagnostics will be used under different conditions. Here are a few examples of photon diagnostics devices, which are already installed in SASE1/3 Beamline and will soon be working:

- X-ray gas monitor detector (XGM) – gas-based detector measuring XFEL pulse intensity and beam position.
- Photoemission spectrometer (PES) – gas-based detector giving information about photon energy spectrum and beam polarization.

- Multi-channel plates (MCP) –shot-to-shot pulse intensity and a spatial image of the beam for both spontaneous and FEL signal.
- K-Monochromator – Undulator studies of k-value.
- Imagers – Beam position studies.
- HIREX- Spectral studies.

2. European XFEL Data Acquisition System "KARABO"

Any complex mechanism requires detail which should coordinate and bring things together. For the European XFEL such thing is a software framework called Karabo. It allows users to control technical infrastructure such as mirrors and optical lasers, acquire information from diagnostics, record and manage data, and do analysis of that data, all with a unified system. All Karabo applications have standardized interface for self-description, program-flow organization, logging and communication. On the other hand it allows simple integration and adaption to changing control requirements and the addition of new scientific analysis algorithms.

As other popular control systems the basic building blocks of Karabo are controllable objects (devices) managed by a device-server. A device-server is a generic application, which loads device-class libraries and communicate via a central message broker. A large set of attributes is available to detail the description of the device properties and commands. Typical attributes for example are: default value, physical unit, displayed label, value-bounds, alarm and warn thresholds, access mode (initially configurable, reconfigurable, read-only), etc.

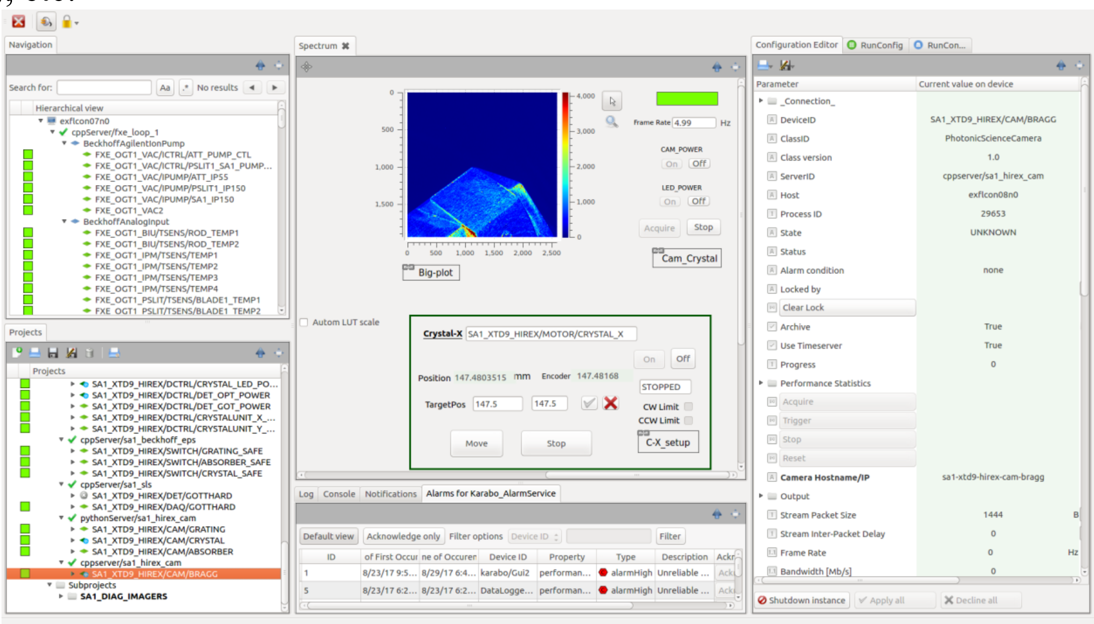

Figure 5: Multi-purpose GUI. Each panel may be unblocked and made full screen on different monitors.

User as an object of device-client can remotely control devices and device-servers, as well as utilized for inquiring the self-description (available properties and commands) of each device. There are five different access levels (rights to make different changes) according to the users' role, IP address of the user and the current time. It is possible to run all Karabo interfaces using either the command line (CLI) or the graphical (GUI) interface. (Figure 5). CL interpreter based on IPython running the device-client, so any interactively given command can as well be written into a regular IPython script and be executed as a macro. Basic layout GUI is formed of seven flexible panels (3):

1. Navigation - real-time overview of the system;
2. Project - project configuration with all components;
3. Notification - informs about warnings, alarms, end-of-runs;
4. Custom - page allowing to build informative working panels from a mixture of online (e.g. device properties and commands) and layout widgets;
5. Logging - logging information of all currently running device;
6. Configuration - properties and commands of the currently clicked devices;
7. Documentation - internet-browser for editing device documentation and bug-reporting;

There are some examples of scenes. Some of this was created to optimize device diagnostics. Others were necessary to facilitate users' interaction with large number of XFEL devices data. (Figure 6)

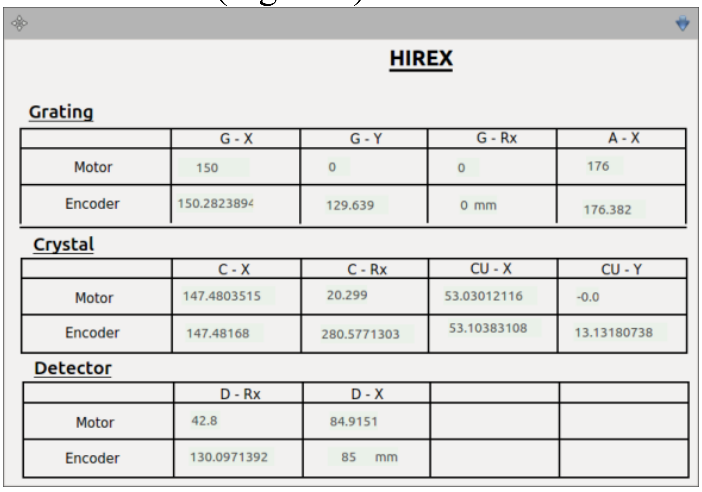

Figure 6: Karabo HIREX motor parameters scene.

3. Dynamic Bender for High Resolution Hard X-ray Single-Shot Spectrometer

3.1 High Resolution Hard X-ray Single-Shot Spectrometer

The HIREX diagnostic spectrometer is an online based device consisted of three units: Grating unit, crystal unit and detector unit. Diamond diffraction grating with pitches of 150nm and 200 nm (4) is used in transmission to split off a small fraction of the photon beam. Then the first order diffracted beam is sent to a bent crystal for energy dispersion under Bragg condition. Two detectors are available for such data acquisition: an optical Photonic Science camera for 2D imaging at low repetition rate, and Gotthard strip detector for MHz-repetition rate. The grating and the crystal chambers are separated by 10 m distance. Various fixed bending radii and crystal reflections cover the hard X-ray range between 3 and 25 keV. Using the XOP 2.4 software (5) is a simple and fast way to figure out different properties and plot the dependencies for crystals with specified parameters. It was used in order to calculate the energy dependence of Bragg angles for different orders and types of reflections, which shown in Figure 7. There are combinations of Miller indices which will give a zero value of a structure factor, thus Darwin width will be also zero. They are forbidden under normal conditions, so you can see no reflection from these crystalline planes.

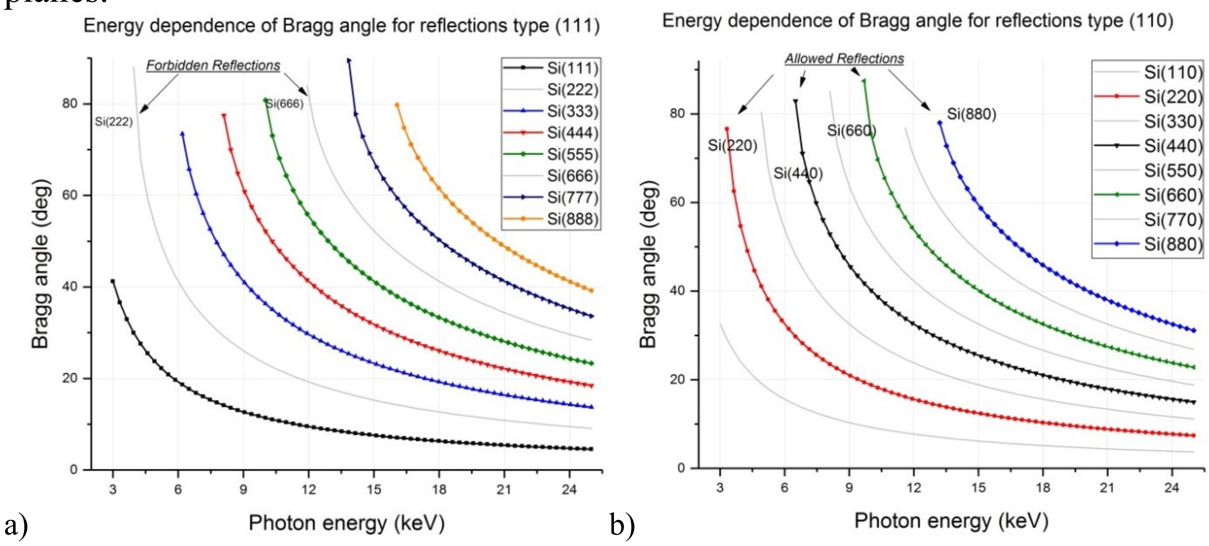

Figure 7: The energy dependence of Bragg angle for reflections type a) Si(111) b) Si(110).

The HIREX spectrometer will provide single-shot spectra for users, whose experiments depend on the knowledge of SASE FEL spectrum (Figure 8). It will provide spectral information to accelerator physicists for machine optimization studies as well. HIREX is installed in XTD9 tunnel for SASE1. Its crystal unit contains a set of four benders of certain radius: 50mm, 75mm, and 100mm. The 10 microns thin Si crystals 20 x 5 mm^2 of (111) and (110) orientations are used for dispersion. (6)

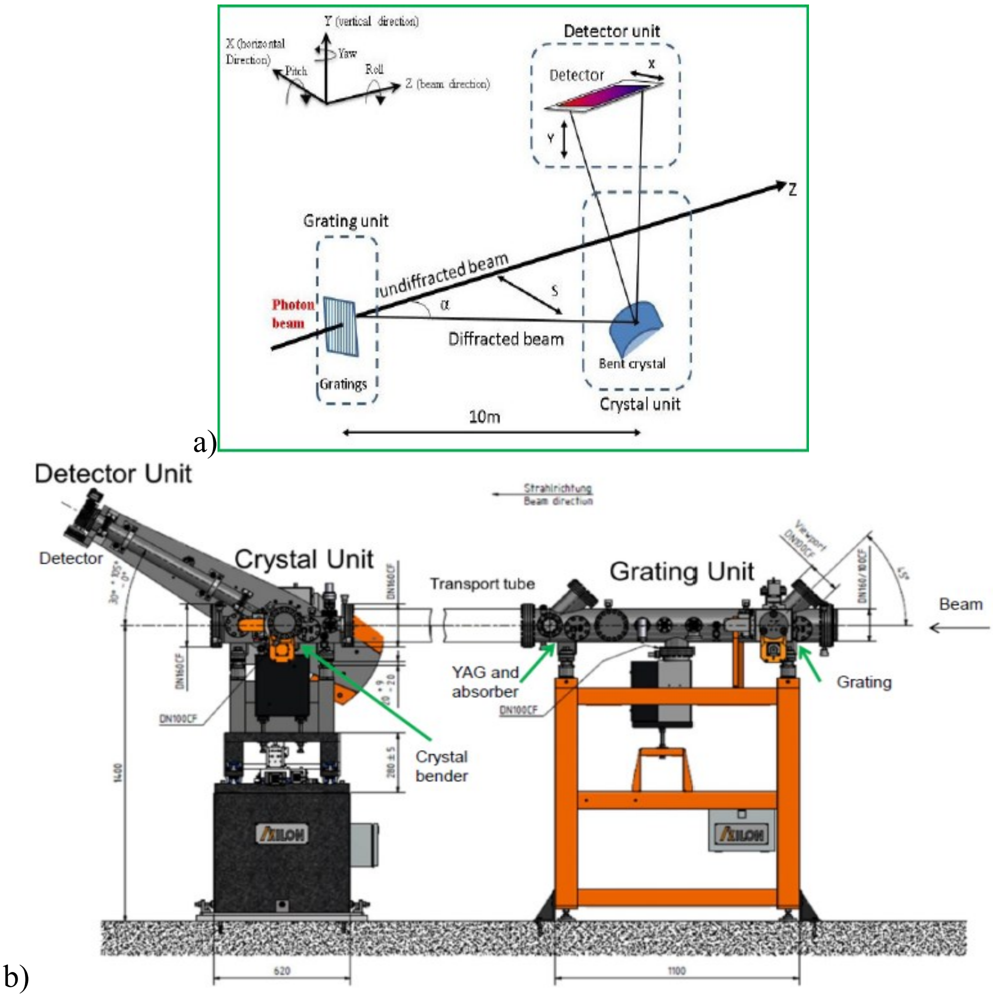

Figure 8: a) Schematic picture of HIREX b) HIREX spectrometer 3D drawing.

In case of the flat crystal due to the Bragg scattering occurs only one certain wavelength separation. However if the wafer is bent convex to the incoming beam, the incidence angle varies over the footprint of the beam in the vertical direction. Therefore, the Bragg law $n\lambda = 2d\sin\theta$ for reflecting lattice planes with spacing d is fulfilled for different wavelengths λ depending on the position on the crystal. Thus the reflections are dispersed in the scattering plane and the diffracted intensities on the different wavelengths could be distinguished. The spectral range of the bent crystal spectrometer, of radius R and X-ray beam width H with the incoming beam energy E and the central Bragg diffraction angle θ_B is: $\frac{\Delta E}{E} = \cot\theta_B \frac{H}{R\sin\theta_B}$. (7)

3.2 Dynamic bender design

The proposed concept for the crystal bender is a holder-pusher principle. Since the silicon crystal is very thin and therefore extremely fragile, it is required to control the clamping force. The crystal could break if the force is too high, or if the screws are tightened not enough the crystal could stay loose. So the lever concept with a spring as shown in Figure 10 a) was chosen to achieve a controlled holding and a crystal replacement without much effort. The lever is held by a cylinder which has on one side a square cross section to prevent it from turning due to the lever movement. Both, ground part and lever do have rounds foreseen, so the fragile sheets do not touch any sharp edges. The holding surfaces was made with a roughness as low as possible.

One more detail that was taken into account is a holding force, which should not be higher than 5 N to avoid damages. The calculations for this were done based on the condition of balance $0 = F_H l_H + F_S l_S - F_{Mass} l_{Mass}$. Here F_S and F_H are spring and holding force respectively. The force of the mass M is $F_{Mass} = gM$ with $g = 9.81 \frac{N}{kg}$ and $M = 0.14\, kg$. The distances $l_H = 16.5\, mm,\ l_S = 11\, mm$ and $l_{Mass} = 8.42\, mm$ are shown in the Figure 10 c) (8).

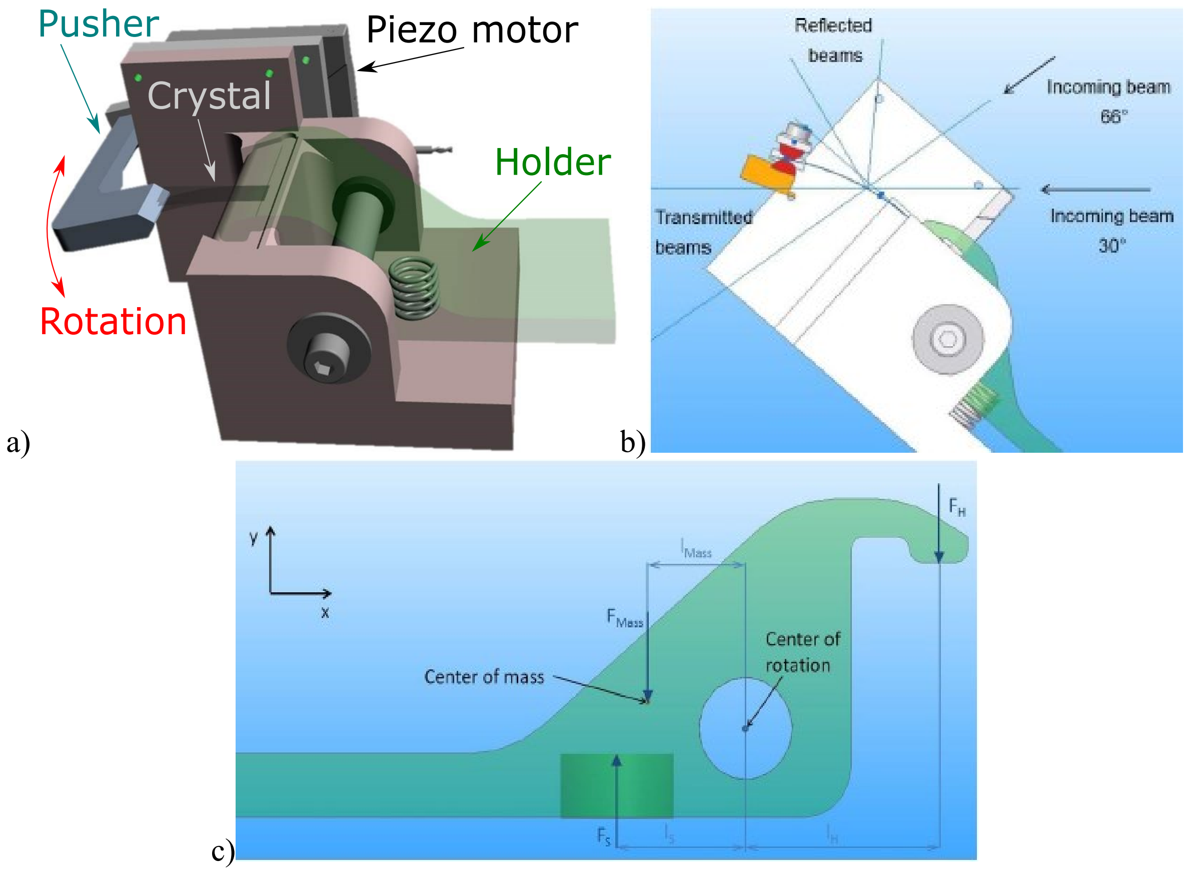

Figure 9: a) Holder-pusher principle. Lever concept with a spring. b) Beam paths depending on the beam energy. The maximum and minimum angles between beam and wafer surface in the point of contact for Si and 5 keV c) Shape of lever with dimensions for calculating the clamping force. (8)

There were several pusher concepts tested. The movement of the free wafer side could be implemented through either linear translation or rotation. The key requirements for the pusher with the driving motor were small size and light weight comparable with parameters of the crystal holder. One of the examples for linear translation approach is slider-driven bending mechanism. To adjust the bending it moves in horizontal plane wedge-shaped stage (9). The disadvantage of this concept is that the wedge angle has to match the local angle of the wafer in a touchpoint for each desired bending radius. Additional requirement for the motor sideway position based on wide spread of incoming, transmitted and reflected beam paths depending on experimental parameters Figure 10 b).

In this research preference was given to the piezo rotation stage mounted at the side. First model had static pusher length arm and two half cylinders with spacer parts fixed with a screw to hold the second side of the crystal. The lower half cylinder is meant to support the wafer end and prevent it from bending due to its own mass. Recently it had been modified, so that it is possible to change the length of the pusher arm. Also there are no extra parts now to hold the free wafer side; however there is a thin slot at the end of the pusher for manipulation with the crystal. These changes should remove the limitations from the plate shape as well as reduce the pressure. The photo of the dynamic bender assembled with clamped 25 µm thin crystals is presented in the Figure 11.

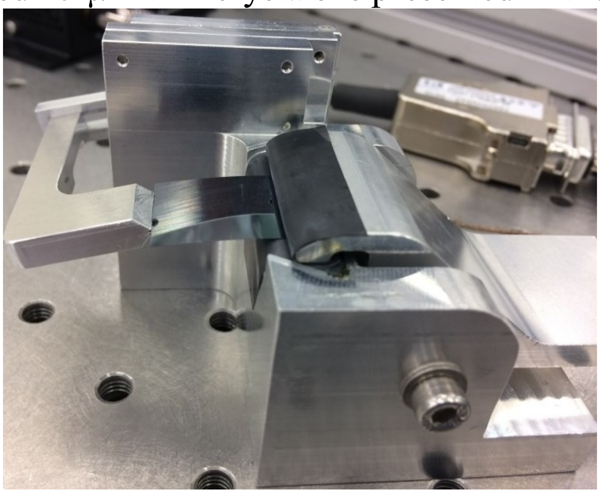

Figure 10: The photo of the dynamic bender assembled with clamped crystal.

3.3 Calculations

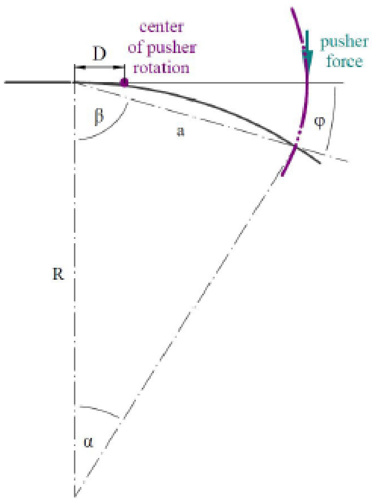

Figure 11: Sketch of the bending geometry. The crystal is seen from the side as thick curve. (8)

To determine the setup geometry, it is necessary to show the relation between the bending radius of the crystal and the rotation angle of the pusher arm. An isosceles triangle shows the expression for the secant $a = 2R\,sin\frac{\alpha}{2}$.

Further expression for the opening angle equals $\alpha = 180 - 2\beta$, while $\beta = 90 - \varphi$. Using the assumption that distance D as shown in Figure 12 is small compared to the radius of the curvature, the equation for bending radius is $R \approx \frac{a}{2\sin\varphi}$. Due to the bender design the average motor step size of the pusher arm is 36 µrad, which equals 2.06 x 10^{-3} °. Since two crystals will be tested: 25µm thin with $a = 25mm$ and 10µm thin with $a = 20mm$ the ratio for them will be slightly different. The corresponding numbers of the motor steps to achieve the specified range of the bender radii for both crystals are shown in tables 1 and 2.

Number of Steps	7027	4657	3485	2320
Angle [°]	14,475	9,593	7,179	4,779
R [mm]	50	75	100	150

Table 1 Theoretical numbers of the motor steps corresponding to achieving the desired bending radii for a=25 µm Si crystal with 25mm length.

Number of Steps	5600	3719	2786	1855
Angle [°]	11,536	7,661	5,739	3,821
R [mm]	50	75	100	150

Table 2 Theoretical numbers of the motor steps corresponding to achieving the desired bending radii for a=10 µm Si crystal with 20mm length.

3.4 Laser results

The pretesting was done using a simple laser point to find out if the bend radii achieved with calculated number of steps and desired ones matches well enough. The laser was set relatively high strictly vertical above the middle region of the bent crystal. To observe the behavior of the reflection a ruler was placed perpendicular to the incidence light. An approximate scheme of the experiment is shown in a Figure 13 complete with a photo as it was looked.

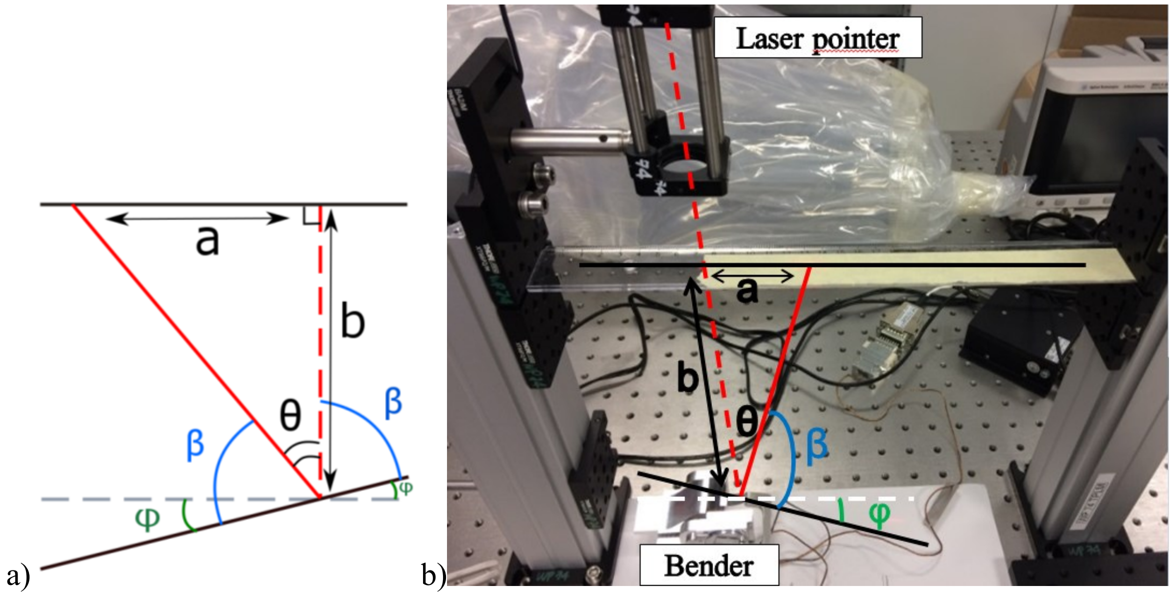

Figure 12: a) An approximate scheme of the experiment b) The photo of the setup with superimposed scheme.

In this simple setup there was one requirement - to align everything. This was important because the spot should go almost along a straight line during the bending process. It is easy to show that the pusher angle is related to the distance traveled by the reflected spot. The angle-to- side ration is obvious $\sin\beta = \frac{a}{b}$ from a right triangle, while the expression for angles ration comes from: $180 - 2\alpha = \beta$ and $90 - \alpha = \varphi$, so $\varphi = \frac{\beta}{2}$. Final equation for this pretesting is: $\varphi = \frac{1}{2}\arcsin\frac{a}{b}$. Thus the idea was to calculate the achieved bend angle through measured spot traveled distance according to the number of motor steps. The collected data and calculated values for both 25 µm and 10 µm thin crystals are presented in the tables 3 and 4. Also dependences of the bend radius from the number of motor steps for 25 µm and 10 µm thin Si crystals are shown in Figure 14.

Number of Steps	2800	3500	3700	4600	5600	7000	8000
a [mm]	37,5	46,5	49,5	63,5	78	99	119
Angle [°]	4,03	4,99	5,32	6,83	8,4	10,68	12,88
R [mm]	178	143	135	105	85	67	56

Table 3 Measured numbers of the motor steps corresponding to achieving the desired bending radii for a=25 µm Si crystal with 25mm length and b=267mm.

Number of Steps	2300	2800	3500	3700	4600	5600	7000	8000
a [mm]	29	33,5	40,5	44	56	70	90,5	106
Angle [°]	3,11	3,60	4,35	4,73	6,02	7,53	9,76	11,45
R [mm]	184	159	132	121	95	76	59	50

Table 4 Theoretical numbers of the motor steps corresponding to achieving the desired bending radii for a=10 µm Si crystal with 25mm length and b=267mm.

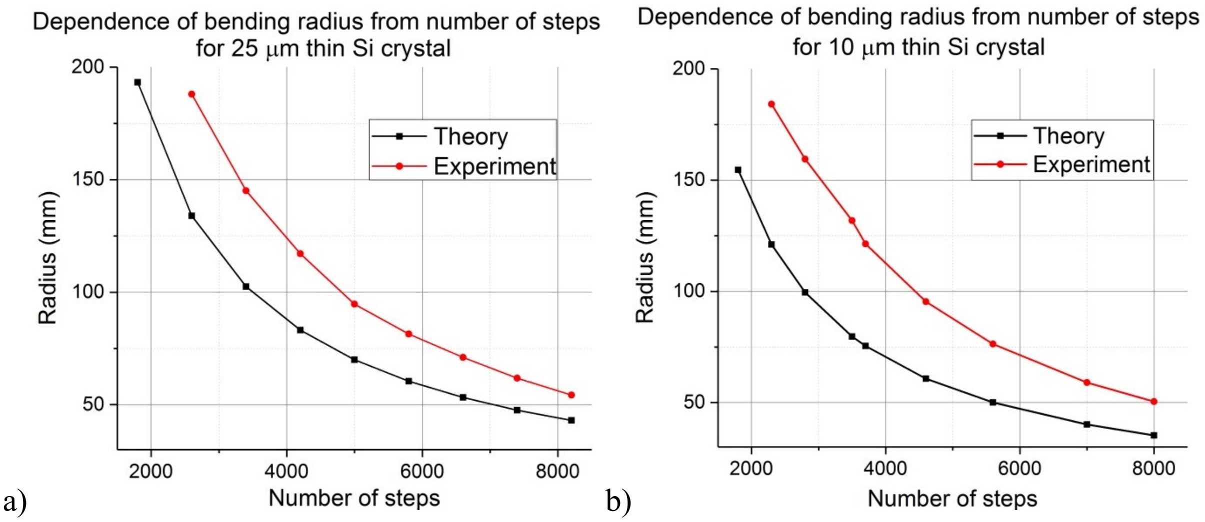

a) b)

Figure 13: Dependences of the bend radius from the number of motor steps a) 25 µm b) 10 µm thin Si crystals.

It was found that the difference between the theoretical values and the experimental is sufficiently large. This could be due to the bending process or fixation of crystal is not uniform. If these assumptions are correct, it is expected that interferometer experiment would show the same error order.

3.5 Interferometer results

The second approach/measurements were performed by white-light interferometry. Incidence beam is splitted by beam splitter; one goes to the sample, another to the perfect mirror. After reflection they go back and then interfere. The fringe displacement depends on the bending radius. Initially, there was a plan to look at the crystal parameters: stress distribution and curvature for four pusher position. Thus it was possible to compare how the actual numbers of motor steps to achieve four desired radii were corresponding to calculate once. Unfortunately, there was a problem faced during the measurements: the interferometer has a requirement that the objective should always be perpendicular to the crystal surface. So the bender doesn't have any goniometer or any mechanism to rotate. That is why the range of the bend radii and period for motor steps was limited with the range of interferometer rotation stages. By this reason the period of motor steps was chosen small that the defocusing could be easily fixed and the smallest observed curve was around 100mm.

At first measurements were carried out with 25 µm Si crystal. The observed x coordinates for holder and pusher crystal sides were 28768 µm and 10611 µm, respectively, hence the length of the bending part was 18 mm. For the flat wafer state was taken the start position with the bend radius of 0,93m. The curve dependence was measured with the period of 100 motor steps in a range from 0 to 2500 motor steps. Also we have tried movements of 150 and 200 steps and reached the technical limit in 3000 steps from flat position and 130m curve. The desired radius of 150mm was achieved by 2400 motor steps, which is almost twice the theoretical value. Error is ranging from 2 to 50%. (Figure 15)

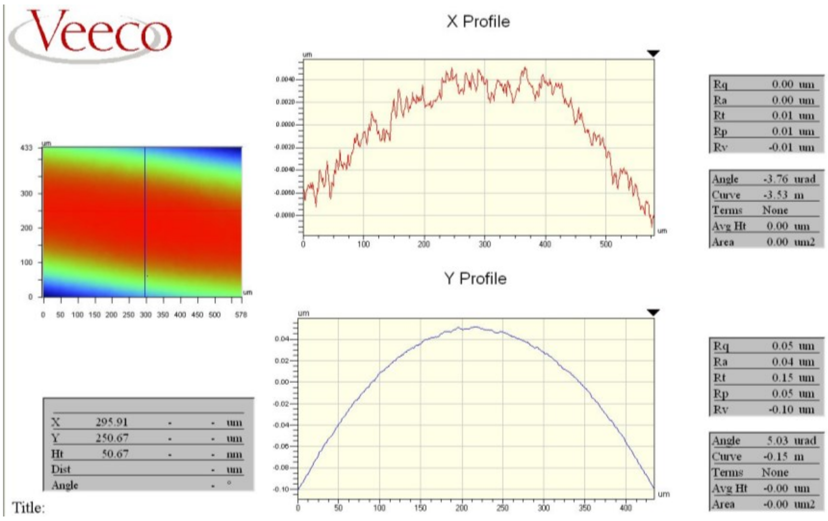

Figure 14: Measurements for 25 µm thin Si crystals with carried out bent radius 150mm and picture of stress distribution dynamic bender.

These results confirm the previously obtained values on the laser and the assumption that bending process has more complex nature. Fortunately the stress distribution throughout the entire bending showed a high degree of uniformity.

Next measurements were carried out with 10 µm Si crystal. The observed x coordinates for holder and pusher crystal sides were 24409.4 µm and 7657.1 µm, respectively, hence the length of the bending part was 16.7 mm. For the flat wafer was taken state with the bent order coincided to noise. As in a previous case the period of measurements was 100 motor steps in a range from 0 to 3100. The technical limit was reached with 150 and 200 steps in 3800 steps from the flat position and 100 mm curve. The desired radius of 150 mm was achieved by 2600 motor steps, what still has a large discrepancy with the calculations.

Some details of the measurements showed important properties of dynamic bender. For first 1500 steps data was taken from the middle of the crystal, however due to the high level of vibrations it was moved to 20% of length from the holder. This shown that the fixation of the wafer is not strong enough, what was mentioned above; also the bending is not evenly along the length (Figure 16).

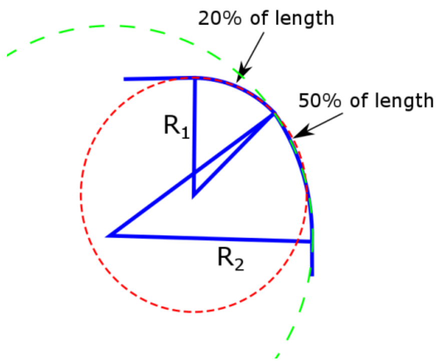

Figure 15: Sketch of the bending geometry carried out from the experiment.

For the main comparison 10 µm Si crystal placed in a static bender unit with an assumed radius 150 mm was measured. This carried out curve equals 160 mm; hence the same curvature state is presented for dynamic bender to compare in Figure 17. As we can see the bent profile (x profile) as well as stress destitution (both x and y profiles) are almost identical.

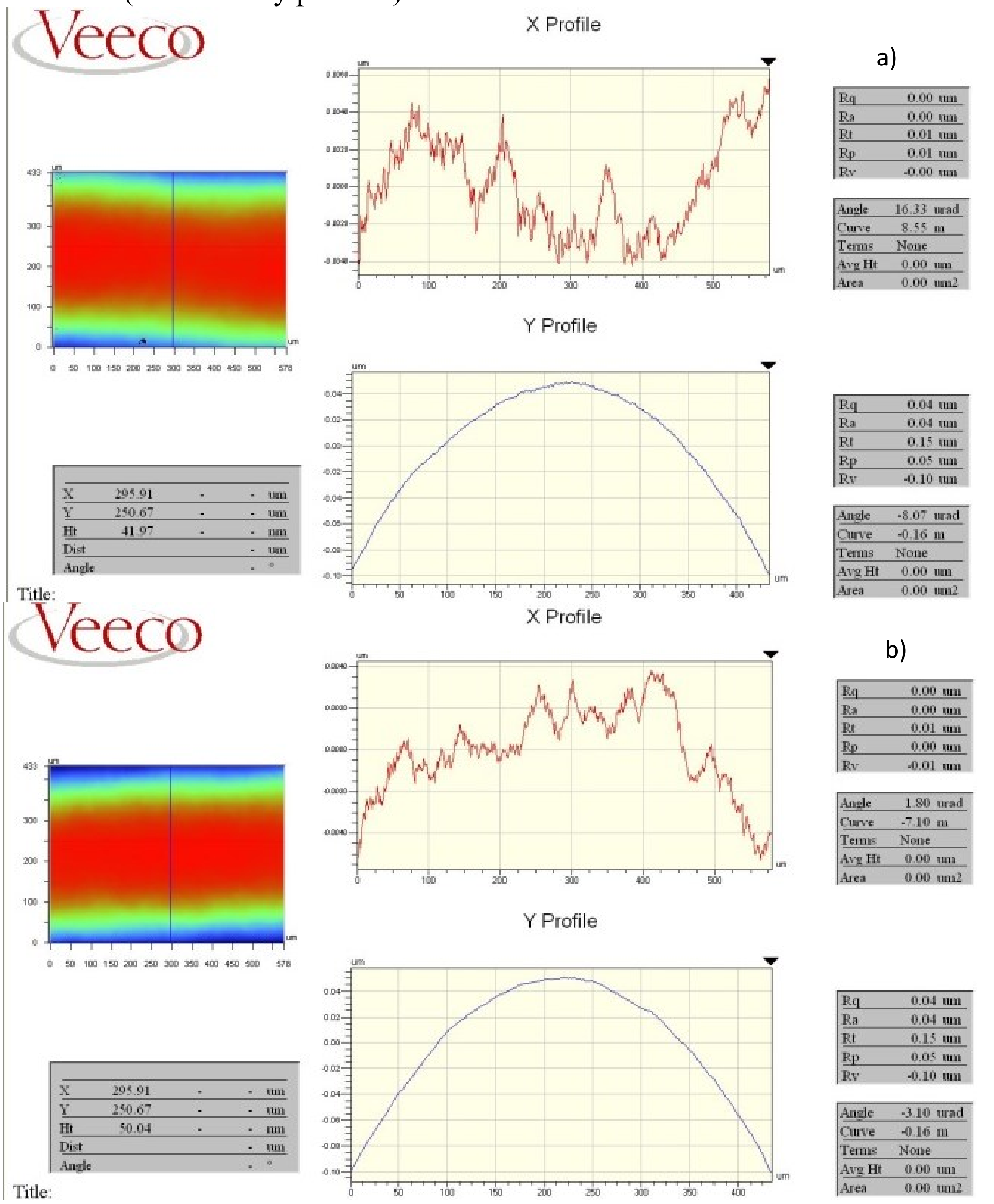

Figure 16 Measurements for 10 µm thin Si crystals with carried out bent radius 160mm and picture of stress distribution a) Static bender unit b) Dynamic bender

4. Conclusion

This research showed that presented dynamic bender in principle could replace the static bend units in high resolution hard X-ray single-pulse diagnostic spectrometer (HIREX). It covers wide range of bending radii at the same time as preserves the uniformity of stress distribution. However for successful work it is necessary to improve technical details of the piezo motor and the pusher arm. Also it would be useful to study the behavior of the bending angle along the length of the crystal during the bending process. In addition the summarized results and challenges for future solution are listed below.

Main results:

- Error between the theoretical and experimental values showed that theoretical model needs to be modified.
- The variety of radii corresponding to different length positions also indicated a more complex character of the bending unlike the model.
-
- It was shown that using the dynamic bender desired radii 50mm, 75mm, 100mm and 150mm could be achieved.
- The stress distribution throughout the entire bending showed a high degree of uniformity.
- Comparison of static and dynamic bent crystals showed the identity of the achieved radii 150mm simultaneously with an equally high degree of stress uniformity.

Problems to be addressed in the future:

- Improve the theoretical model.
- Improve the technical characteristics of the dynamic bender.
- Compare different length positions for static and dynamic bent crystal.
- Carry out measurements with a bigger field of view.

5. Acknowledgement

I would like to thank my supervisor Dr. Naresh Gandhi Kujala for the support throughout this project. Thanks to him, I was lucky to see many aspects of the work both at DESY and at XFEL. This research would also be impossible without support from Birthe Kist, who allowed to use the bender for modify. I would also like to thank the Photon Diagnostics group for friendly atmosphere and assistance in solving problems. During my study of Karabo I was strongly supported by Ehsan Wajid from Control & Analysis Software group. Also I would like to express my gratitude for Idoia Freijo Martin and Maurizio Vinnoni from X-ray Optics & Beam Transport group for spending their time on interferometer data taking.

I thank the DESY summer student organizing team for running this program and making this opportunity possible.

6. Bibliography

1. *Photon Beam Transport and Scientific Instruments at the European XFEL.* **Thomas Tschentscher, Christian Bressler, Jan Grünert, Anders Madsen, Adrian P. Mancuso,.** s.l. : Applied science, 2017.

2. *Framework for X-ray Photon Diagnostics at the European XFEL.* **Jan Grünert.** 2012.

3. *Karabo: An integrated software framework combining control, data management, and scientific computing tasks.* **B. C. Heisen, D. Boukhelef, S. Esenov, S. Hauf, I. Kozlova, L. Maia, A. Parenti, J. Szuba, K.Weger, K. Wrona, C. Youngman.** s.l. : ICALEPCS, 2013.

4. *Fabrication of diamod diffraction grating for experimants with intense hard X-rays.* **Mikako Makita, Petri Karvinen, Vitaliy A Guzenko, Naresh Kujala, Patrik Vagovic, Christian David.** s.l. : Microelectronic Engineering, 2017.

5. *XOP: A graphical user interface for spectral calculations and X-ray optics utilities".* **Roger J. Dejus, Manuel Sanchez del Rio.** s.l. : Rev. Sci. Instrum., 1996.

6. *Photon diagnostics and photon beamline installations at the European XFEL.* **Jan Grünert, Andreas Koch, Naresh Kujala, Wolfgang Freund, Marc Planas, Florian Dietrich, Jens Buck, Jia Liu, Harald Sinn, Martin Dommach, Serguei Molodtsov.** s.l. : Proceedings of FEL, 2015.

7. *High-resolution single-shot spectral monitoring of hard X-ray free-electron laser radiation.* **M. Makita, P. Karvinen, D. Zhu, P. N. Juranic, J. Grünert, S. Cartier, J. H. Jungmann-smith.** s.l. : Optica, 2015.

8. *Design of a Crystal Bender for a Spectrum Analyser at the Materials Imaging and Dynamics beamline of the European X-ray Free Electron Laser.* **Birthe Kist.** s.l. : BA thesis, 2015.

9. *X-ray spectrometer based on a bent diamond crystal for high repetition rate free-electron laser applications.* **Ulrike Boesenberg, Liubov Samoylova, Thomas Roth, Diling Zhu, Sergey Terentyev, Maurizio Vannoni, Yiping Feng, Tim Brandt van Driel, Sanghoon Song, Vladimir Blank, Harald Sinn, Aymeric Robert, Anders Madsen.** s.l. : Optical Society of America, 2017.